Surfactant and dopant addition effect on optical and structural properties of ZnSe (Te) nanostructured semiconductors

Lucas G. Valluzzi, Marcos G. Valluzzi, Germán N. Darriba, Marcos Meyer, Laura C. Damonte

PII: S0925-8388(20)30851-3

DOI: https://doi.org/10.1016/j.jallcom.2020.154488

Reference: JALCOM 154488

To appear in: *Journal of Alloys and Compounds*

Received Date: 2 January 2020

Revised Date: 15 February 2020

Accepted Date: 22 February 2020

Please cite this article as: L.G. Valluzzi, M.G. Valluzzi, Germá.N. Darriba, M. Meyer, L.C. Damonte, Surfactant and dopant addition effect on optical and structural properties of ZnSe (Te) nanostructured semiconductors, *Journal of Alloys and Compounds* (2020), doi: https://doi.org/10.1016/j.jallcom.2020.154488.

CRediT author statement

Lucas G. Valluzzi: Data curation, Investigation, Formal Analysis, Writing- Original draft preparation.

Marcos G. Valluzzi: Data curation, Investigation.

Germán Darriba: Ab initio calculation, Writing- Reviewing.

Marcos Meyer: Data curation, Software, Validation, Visualization, Writing- Reviewing and Editing.

Laura C.Damonte: Conceptualization, Methodology, Writing- Reviewing and Editing, Supervision, Project Administration

Surfactant and dopant addition effect on optical and structural properties of ZnSe (Te) nanostructured semiconductors

Lucas G. Valluzzi[1], Marcos G. Valluzzi[1], Germán N. Darriba[2], Marcos Meyer[2] and Laura C. Damonte[2]

[1] IDEI, Universidad Nacional de Tierra del Fuego (UNTDF)

[2] Dto. de Física, Facultad de Ciencias Exactas, UNLP-IFLP, CCT, CONICET

Abstract

ZnSe and ZnTe nanoparticles were obtained by mechanical milling. The influence of surfactant and doping agent addition on structural and optical properties were analyzed. X-ray diffraction (XRD) confirmed cubic crystalline structure is maintained for all milling times and the progressive substitutional incorporation of Al atoms into the Zn-based semiconductor structure.

The agglomerate state of milled powders was disclosed by scanning electron microscopy (SEM), and Dispersion Light Scattering (DLS). Positron annihilation lifetime (PALS) spectroscopy allowed to identify the defects induced by mechanical work. A slight shift on the energy band gap with respect to pure semiconductor nanoparticles was revealed from optical diffuse reflectance measurements for all studied samples. The obtained results agree with first-principles calculations based on the Density Functional Theory (DFT). The calculations predict that Al substitute the Zn atom in the ZnTe and ZnSe lattice and a zinc vacancy must appear in order to recover the semiconductor character, as shown (or suggest) the experimental results. The characteristic positron annihilation lifetimes for the doped samples are obtained for both systems and compared with those measured. This theoretical approach helps us to deeper understand the origin and characteristics of different positrons traps.

Keywords: Zn-based nano particles; optical properties; positron annihilation; open volume defects, first principle calculations

1. Introduction

Zinc Selenide (ZnSe) and Zinc Telluride (ZnTe) are important II-VI semiconductor materials with direct and wide band gap (2.82 eV-2.26 eV). These materials have many potential optoelectronics applications, such as photo detectors, solar cells, lasers [1-11]. A long range of techniques have been used to fabricate these materials as electrochemical deposition [5], molecular beam epitaxy (MBE) [2], mechanical ball milling and others [8, 10]. The performance of the different devices may be improved enhancing their characteristic properties which can be attained by increasing interfacial processes or dopant addition. Nowadays, nanocrystalline materials seem to be the best option to reach this goal. In this sense, thin films [4, 12], nanorods [13-14], nanosheets [2, 15], nanowires [16-17], etc. have proved this statement. In addition, solid state reaction techniques, like mechanical milling [18] have also been applied to obtained nanoparticles, quantum dots and doped semiconductors [8, 10, 19-22]. However, one disadvantage of this synthesis method is particles agglomeration and cold-welding producing increase particle sizes during ball milling operations. In order to avoid these problems is necessary the use of surfactants such as methanol, ethanol, Zinc chloride and others [10].

In a previous work, we have investigated the effect of milling time on pure ZnSe and ZnTe semiconductor powders [21] by means of X-ray diffraction (XRD) and Positron Annihilation Lifetime Spectroscopy (PALS). These preliminary results indicated grain size reduction as milling proceeds and the formation of a diversity of defects. Al addition on ZnTe semiconductor using PALS, XRD and X-ray absorption fine structure (XAFS) was investigated in a subsequent work confirming the dopant incorporation in the crystalline structure of ZnTe [22].

In this opportunity, methanol and Zinc chloride were incorporated as surfactants during milling and the effect of doping agent on the structural and optical properties of Zn-based semiconductors is analyzed. Structural characterization of all the prepared powders was performed by X-ray diffraction, Scanning Electron Microscopy (SEM), Dispersion Light Scattering (DLS) and Positron Lifetime measurements (PALS). The changes on optical properties were evaluated measuring the diffuse reflectance by UV-vis spectroscopy. Undoped ZnSe and ZnTe nanocrystalline powders prepared in a similar way were analyze for comparison.

We complement the experimental data using a strategy previously developed [23] based in very accurate and precise theoretical *ab initio* calculation of positron lifetimes in solids in the framework of the Density Functional Theory (DFT). In this approach the equilibrium structures of the doped systems (i.e., final atomic positions) were obtained applying the Full-Potential Augmented Plane Wave plus local orbitals (FP-APW+lo) method [24], embodied in the WIEN2k code [25]. The Multigrid Instead of the K-spAce (MIKA) program [26] was then used to predict the characteristic semiconductor lifetimes at these equilibrium structures. Also, in order to evaluate the effects in the lifetime produced by the structural relaxations, we predict the annihilation lifetimes for the non-relaxed systems. With the aim

to elucidate electronic distortions introduced by the different defects (Al substitutional, Zn vacancies) in the semiconductor the electronic density of states (DOS) were evaluated.

The joint experimental and theoretical analysis will allow us to a better comprehension on the structural and optical properties of these semiconductors towards their potential applications.

2. Experimental

Un-doped and Al doped ZnSe and ZnTe nanopowders were obtained by mechanical milling in a Retch MM2 horizontal vibratory mill. The starting materials were ZnSe (99.99%) and ZnTe (99.99%) powders from Aldrich Chemistry (Sigma-Aldrich Co.) and Al_2O_3 (99.99%) powders from Alfa Aesar (Johnson Matthey Co.). The doped samples were prepared by mixing stoichiometric quantities to obtain 5 at % Al.

The mechanical milling was performed in air atmosphere at a frequency of 30 Hz for different milling times (1, 10 and 30 hours). The ball to powder mass ratio was 10/1 using a steel cylinder (8 cm^3) with one steel ball (diameter 12 mm). To avoid agglomeration effect on the final product, millings with two surfactants, methanol or $ZnCl_2$, were also done.

X-Ray Diffraction (XRD) characterization was performed using a Philips Diffractometer (PW 1732/10 Generator and PW1050/70 Goniometer), Holland. X-rays Tube PW 1710 with Cu K_α (λ=1.5406 Å), with a nickel filter. The work conditions were: 40 KV and 20 mA, scan rate 0.25 º/min, step 0.02 and angular range $20° < 2\theta < 80°$.

Particle size distribution of milled powders was determined by Dispersion Light Scattering measurements (DLS). For this purpose, the milled powders were suspended in methanol at a concentration of 0.5 mg/ml and homogenized in an ultrasonic bath for 15 to 45 minutes.

DLS equipment consists basically in a *He-Ne* Laser and a photometer that measures the scattered light intensity from the sample at an angle of 90° with respect from the incident laser beam direction, then the autocorrelation function of scattered light intensity at different times was calculated.

The surface morphology of the samples was studied using scanning electron microscopy (SEM) in a Philips SEM 505 microscope. The atomic percent compositions (say at%) of the samples were obtained from EDAX ZAF Quantification using an SDD Apollo X detector.

Positron annihilation lifetime (PALS) measurements were done with the aim to characterize the mechanical induced defects. The milled powders were hydrostatically pressed into 8 mm diameter pellets. PALS measurements were performed at room temperature in a conventional fast-fast coincidence system with two scintillator detectors yielding a time resolution (FWHM) of 250 ps. The positron source, 10 μCi ^{22}NaCl, deposited onto a kapton foil (1.42 g/cm^3), was sandwiched between two sample pieces. The source contribution and the response function were evaluated from a Hf metal reference sample using the RESOLUTION code. Positron lifetime spectra of at least 3 x 10^6 counts each were analyzed with the POSITRONFIT program [27]. A PALS spectrum, n(t), consists of a histogram of measured annihilation times of individual positrons in the material formed by several exponential decay components, each with a different intensity and lifetime (I_i, τ_i), convoluted with the instrumental resolution of the detection system (response function) and subject to experimental background:

$$n(t) = \sum_i I_i e^{-t/\tau_i} \qquad (1)$$

The positron annihilation rate λ_i in a state i is proportional to the electron density at the site of the positron. These parameters are related with the lifetime components as:

$$\lambda_i = 1/\tau_i \qquad (2)$$

The state in question can be the delocalized state in the lattice or the localized state at a vacancy type defect.

Optical characterizations were carried out by diffuse reflectance spectroscopy on the powder pellets. All spectra were taken in the range of 200-1100 nm using a Shimadzu 2600 UV-vis spectrophotometer with integrating sphere attachment ISR-2600 Plus.

3. Results and Discussion

3.1 X-Ray Diffraction (XRD)

XRD patterns for ZnSe and ZnTe powders, after different milling times, with and without surfactant and doping agent are shown in Figure 1 and Figure 2, respectively.

All of them display the reflection lines of cubic (F43m) for ZnSe or ZnTe. It can be observed that in the case of ZnSe, the surfactant addition induces peak broadening, consequence of grain size reduction (figures 1 b and c). Instead, in the case of ZnTe the broadening of diffraction peaks with increasing milling time is less marked than in ZnSe (figure 2).

It is worthwhile to note that no trace of oxide compounds nor segregation is observed within the technique resolution [8].

Rietveld´s refinement method with Thompson–Cox–Hastings pseudo-Voigt profiles was applied to determine structural type, lattice parameters and Coherent domain size $L[nm]$, using Fullprof Software. Tables 1 and 2 display the results obtained for ZnSe and ZnTe,

respectively. It can be observed for ZnSe that the use of surfactant ($ZnCl_2$ or methanol) after prolonged milling time reduces the coherent domain size between 10-15% the value obtained without surfactant. However, in the case of ZnTe samples, surfactants do not produce a different effect as 10h of milling without surfactant (Table 2).

The Al doped samples were milled without surfactant. Figures 1d and 2d show the corresponding diffraction patterns for doped ZnSe and ZnTe, respectively, where a similar feature to the un-doped sample can be observed. The crystalline structure (cubic F43m) remains the same for all milling times and no reduction of grain size is observed with evolution time (Table 1 and 2).

Milling produce an increasing in the lattice parameter for all samples (Table I and II) This result cannot be assigned exclusively to the incorporation of Al into the ZnSe or ZnTe lattices because it also occurs in undoped samples. In addition, the ionic radius of Al is smaller than the ionic radius of Zn. Then such increase is due to the generation of defects introduced by grinding.

Table 1. *Sample details, Rietveld results for coherent domain length, particle size distribution (obtained from DLS analysis), and Lattice parameter (absolute and relative) for ZnSe powders.*

System	***Milling Time (h)***	***Surfactant***	***Coherent Domain Length (nm)***	***Centered Size Distribution (nm)***	***Lattice Param a (Å)***	***Δa/a (x10^{-3})***
$ZnSe$	10	*No*	140_3	220_5	5.665_5	*8.36*
$ZnSe$	1	$ZnCl_2$	150_3	-	5.647_4	*5.16*
$ZnSe$	10	$ZnCl_2$	120_3	190_5	5.718_5	*17.8*
$ZnSe$	30	Methanol	130_3	170_5	5.642_5	*4.27*

$ZnSe(Al)$	1	No	*150_3*	-	*5.646_4*	*4.98*
$ZnSe(Al)$	10	No	*150_3*	*165_5*	*5.624_6*	*1.07*
	10		*140_4*	*170_5*	*5.661_5*	*7.65*

Table 2. *Sample details, Rietveld results for coherent domain length, particle size distribution (obtained from DLS analysis), and Lattice parameter (absolute and relative) for ZnTe powders.*

System	***Milling Time (h)***	***Surfactant***	***Coherent Domain Length (nm)***	***Centered Size Dsitribution (nm)***	***Lattice Param a*** *(Å)*	***Δa/a*** ***($x10^{-3}$)***
$ZnTe$	10	*No*	*190_3*	*230 to 300*	*6.092_4*	*3.62*
$ZnTe$	1	$ZnCl_2$	*200_3*	-	6.096_5	4.28
$ZnTe$	10	$ZnCl_2$	*190_3*	*200 to 300*	*6.104_5*	*5.60*
$ZnTe$	30	Methanol	*185_3*	-	6.123_6	8.73
$ZnTe(Al)$	1	No	*200_3*	-	6.086_5	*2.63*
$ZnTe(Al)$	10	No	*200_3*	-	6.089_6	*3.13*

3.2 Scanning electron microscopy (SEM)

All the samples have similar morphology aspect SEM images, showing an agglomeration of fine particles. Figure 3 shows the obtained SEM image for the Al:ZnSe 10 h milled sample. ~~The~~ EDAX analysis was performed to checked doping concentration yielding an Al concentration between 4,5 and 5 at% for all cases. Also, a slight iron contamination in the largest milling times, coming from milling tools was revealed. This contamination takes the major value for Al:ZnTe (1.5 at%), but is low enough to be detected by XRD.

3.3 Dynamic Light Scattering (DSL)

Dynamic Light Scattering was applied to obtained particle size and their distribution on those samples with prolonged milling times. The data were analyzed by Mie theory with different proposed models according to the resulting distribution [28]. For a monodisperse size distribution the cumulant method, which gives the average ratio (R) and the polydispersity index (PI), was used. On the other hand, if the particle size distribution results polydisperse, a different analysis providing information on intensity, mass or number distribution must be performed. In both cases, a nanoparticle spherical model is assumed.

The obtained results on particle size distribution for both systems are also summarized in Tables 1 and 2.

The measurements proceeded only with the part of sample that remain in the suspension. The rest of sample that precipitate is not measured at all. In the case of ZnTe milled with or without surfactant could not be measured due to null contrast.

From these results it can be observed that no deagglomeration could be achieved and the use of surfactant yields no major change. Since the centered size distribution (nm) obtained from DLS measurements are of the same order of magnitude than the coherent domain length (nm) resulting from Rietveld analysis, it can be concluded that these samples are monocrystalline.

3.4 Positron Annihilation Lifetime Spectroscopy (PALS)

In order to characterize the defects induced by mechanical work Positron Annihilation Lifetime Spectroscopy (PALS) technique was applied.

The lifetime spectra were decomposed into three exponential decays according to equation (1) being the parameters that characterized each positron state, i.e. the annihilation rate $\lambda_i = 1/\tau_i$ and its relative intensity I_i, obtained by the POSITRONFIT fitting program [27].

Normally, II-VI semiconductor compounds exhibit two-lifetime components spectra since intrinsic and extrinsic defects (such as vacancies, interstitials, etc.) usually introduced during crystal growth and doping are unavoidable [18]. The shorter component (τ_1) comes, usually, from free annihilation of positrons in the delocalized bulk state and the other (τ_2) from trapped positrons at defects. The longest component τ_3 is ascribed to ortho-positronium annihilation formed in large voids present in the material or in the surrounding of the source. In the present study, this component (1700 to 1900 ps) maintains its low intensity I_3 around 3% in all the analyzed samples, so it will not be considered in the forthcoming discussion. Since in this instance, no source correction was previously assumed in the fitting procedure, positron annihilation at kapton foil (15% of a lifetime of 386 ps) must be included in the second component. A typical PALS spectrum (corresponding to pure ZnSe) is shown as inset in figure 4 and the annihilation parameters obtained from fitting procedure are shown in Table 3.

For pure samples (ZnTe and ZnSe), the first lifetime component, associated to positron annihilation in bulk material, agrees with reported values [29]. The second one has lifetimes and intensities higher than the ones observed for single crystals, which indicates positron trapping at different intrinsic defect as is usually observed in semiconductor materials. During mechanical milling, the powders suffer severe plastic deformation giving rise to particle and grain refinement. Different kinds of defects, such as vacancies, vacancy clusters, dislocations, etc., are simultaneously created.

For the powders milled with different surfactants and doping agent (Al) this process is more evident giving place to an increase in both lifetime contributions and their relative intensities. The first positron lifetime rises about a 20% respect its value for the pure semiconductor, which indicates the presence of monovacancies, divacancies or interstitial atoms.

The ratio of the defect related lifetime to the bulk lifetime, τ_D/τ_B, can be used to estimate the relative amount of open volume of the defect. A ratio of less than 1.2 is typical for a monovacancy defect, whereas a ratio of 1.25-1.45 is typical for a divacancy defect [29]. Assuming bulk lifetimes of 233 ps for ZnSe and 257 ps for ZnTe, the ratio $\tau_D/\tau_B > 1.55$ (Table 3), where the obtained second lifetime was considered as τ_D. These large values mean that the open volume defects present in these samples are larger than a vacancy or otherwise a variety of defects with similar positron lifetimes are contributing to the second lifetime component. If the last is the present case, the lifetimes of all these point defects are unable to be separated, so we have evaluated the average positron lifetime. This parameter can be calculated as the sum of individual lifetime components, weighted with the normalized intensity of each component as:

$$\tau_{AVE} = \sum_{i=1}^{N} I_i \tau_i \Big/ \sum_{i=1}^{N} I_i$$

The increase of the average lifetime above the positron lifetime in bulk indicates vacancy-type defects presence [19-22, 30]. In figure 4 the average lifetime for all the analyzed samples is displayed, showing the clear presence of open volume defects.

Table 3*. Positron annihilation parameters.*

Sample	$\tau_1(ps)$	$I_1(\%)$	$\tau_2(ps)$	$I_2(\%)$	τ_D/τ_B	$\tau_{ave}(ps)$
ZnSe 5% Methanol	282_{19}	48_{15}	411_{26}	48_{15}	1.76	333
ZnSe 3% $ZnCl_2$	263_{25}	33_{14}	393_{18}	64_{14}	1.69	338
ZnSe 5%Al	280_{16}	47_{12}	415_{20}	50_{12}	1.78	339
ZnSe	199_{10}	42_{4}	386_{9}	56_{4}	1.66	300
ZnTe 5% Methanol	302_{16}	54_{15}	423_{25}	43_{15}	1.64	345
ZnTe 3% $ZnCl_2$	340_{14}	80_{14}	490_{8}	17_{14}	1.90	355
ZnTe 5%Al	255_{13}	32_{6}	412_{9}	64_{6}	1.60	345
ZnTe	199_{12}	32_{3}	407_{9}	63_{3}	1.58	317

3.5 UV-vis Spectroscopy

Optical characterization was carried out by measuring the diffuse reflectance on the powder pellets. The resulting absorption spectra were obtained using the Kubelka-Munk (K-M) model available in the UV Probe software provided with the spectrophotometer. The effect on optical properties of surfactant and dopant addition is shown in Figure 5. A clear different behavior for each semiconductor can be observed. The influence of surfactant amount and kind was analyzed for ZnSe, which results are shown in figure 5a. Broad and strong absorption profiles in the UV-vis (200-500 nm) region of electromagnetic spectrum are observed, resulting a reduced absorption value when methanol is used as surfactant. The ZnTe samples are characterized by an abrupt absorption edge in the UV region with similar absorption values for pure, doped and surfactant milled samples.

According to Tauc−Mott theory, the photon energy ($h\nu$) dependence of the absorption coefficient (α) can be described as [31]:

$$\alpha h\upsilon = B\,(h\upsilon - E_g)^{n} \quad (5)$$

where B is a constant, E_g is the band gap energy of the material and n is an index that characterizes the optical absorption process (for a semiconductor material with direct band gap n = ½). Therefore, the band gap energy of these powders can be estimated from a plot of $(\alpha h\nu)^2$ versus $h\nu$, extrapolating the linear part of the graph (Figure 6) until it meets the x-axis. Then, the values obtained are in the range 1.3-1.7 eV for ZnSe and 1.3-2.1 eV for ZnTe samples. These values are lower than the reported energy band gap for bulk samples (2.82 and 2.26, respectively). It is known that optical band gap depends on preparation method, morphology and defects presence [8, 12, 14-17, 32]. In our case this red shift can be due to the presence of open volume defects as it was stated by PALS results. Moreover, from figure 6 it can be appreciated some ripples which may indicate the energy absorption from defect states. In all cases the measurement of a band gap indicates the semiconductor behavior for the analyzed samples. These results are consistent with structural and morphological studies where other authors reported that the band gap shift depends on the existence of intrinsic defects, the density of dislocations and quantum size effect [15-16].

3.6 Ab initio calculations

In order to get an insight on the optical and electronic properties some preliminary ab-initio calculations were done.

We present here the electronic structure DFT-based *ab initio* calculations in Al-doped ZnSe and ZnTe semiconductors. The ZnSe and ZnTe unit cells have a zinc-blende cubic geometry (space group *F-43m*), with *a*= 5.668 Å for ZnSe and *a*= 6.101 Å for ZnTe. The ZnSe unit

cell contains 4 Zn and 4 Se atoms, while the ZnTe unit cell contains 4 Zn and 4 Te atoms. To simulate the Al-doped systems, the calculations were performed replacing one Zn atom by one Al atom in ZnSe (called ZnSe_AlxZn) and in ZnTe (called ZnTe_AlxZn). Also, we performed calculations replacing one Se atom by one Al atom in ZnSe (called ZnSe_AlxSe) and replacing one Te atom by one Al atom in ZnTe (called ZnTe_AlxTe). As we will show, the generation of a Zn vacancy (V_{Zn}) together with the substitution of a Zn by an Al atom (AlxZn) is necessary to reproduce the semiconductor character of the systems. Therefore, we performed *ab initio* calculations generating Zn vacancies in the pure and in the Al-doped ZnSe and ZnTe semiconductors. We called ZnSe_V_{Zn} and ZnTe_V_{Zn} when one Zn atom is removed from ZnSe and ZnTe, respectively. For the Al-doped systems, we called ZnSe_AlxZn+ V_{Zn} and ZnTe_AlxZn+ V_{Zn} when one Zn atom is removed from the ZnSe_AlxZn and ZnTe_AlxZn systems, respectively. In order to simulate the different concentrations (1/4, 1/8, 1/16 and 1/32) of Al impurities and Zn vacancies we used the unit cell and a 2x2x2 supercell (SC) containing 4 unit cells of ZnSe or ZnTe (i. e., 32 Zn and 32 Se atoms, and 32 Zn and 32 Te atoms for the ZnSe and ZnTe SC). For 1/4 dilution of the Al impurity we replace 1 Zn atom for 1 Al in the unit cell. For the 1/8, 1/16 and 1/32 dilutions we replace 4, 2 and 1 Zn atoms for 4, 2 and 1 Al atoms in the 2x2x2 SC, respectively. The same criteria but removing Zn atoms instead of replacing by Al atoms, was used to simulate the different concentrations (or dilutions) of Zn vacancies.

To obtain the electronic structure at the final atomic equilibrium positions in Al-doped ZnSe and ZnTe, and Zn vacancies in ZnSe, ZnTe, and Al-doped ZnSe and ZnTe systems we performed a complete optimization of all atoms in the SC (relaxed structures). We employed the FP-APW+lo methods [24] embodied in the WIEN2k code [25]. The local-density approximation (LDA) and the generalized gradient approximation (PBE-GGA) was used to

treat the exchange and correlation effects, obtaining basically the same final atomic positions with both approximations. The cut-off parameter of the plane wave bases in the interstitial region was $R_{MT}K_{max}=7$, where R_{MT} is the smallest radius of the non-overlapping muffin-tin spheres centered in the atoms, and Kmax is the maximum modulus of the lattice vectors in the reciprocal space. In our calculations we use R_{MT}(Zn)=1.21 Å, R_{MT}(Te)= R_{MT}(Se)= 1.16 Å and R_{MT}(Al)= 1.00 Å. The integration in the reciprocal space was performed using a *k*-space gird of 9x9x9.

The positron annihilation lifetime τ was predicted for both, the unrelaxed structure and for the relaxed structures predicted by WIEN2k, using the MIKA/Doppler program [26], based in the atomic superposition method [33]. As shown in a previous work [23] we check that using the LDA approximation and treating the electron density enhancement factors at the positron as proposed by Boronski and Nieminen (BN) [34] the more accurate predictions were obtained.

The electronic structure and τ were also predicted for the pure (undoped) ZnSe and ZnTe systems, to evaluate the effects produced by the different defects.

The substitution of a Zn atom by an Al one as well as the generation of Zn vacancies causes strong changes on the electronic structure of both ZnSe and ZnTe semiconductors. In Figure 7 we compare the electronic density of states (DOS) of undoped ZnSe and ZnTe with those corresponding to Al-doped (ZnSe_AlxZn, ZnSe_AlxSe, ZnTe_AlxZn, and ZnTe_AlxTe) and with Zn vacancies, both in the undoped (ZnSe_V_{Zn} and ZnTe_V_{Zn}) and Al-doped (ZnSe_AlxZn+V_{Zn}, and ZnTe_AlxZn+V_{Zn}) ZnSe and ZnTe semiconductors.

In all cases, the DOS corresponds to the relaxed systems, i. e., after finding the final atomic equilibrium positions and considering the displacement of all the atoms of the SC. For both pure semiconductors, the replacement of a Zn atom by an Al one introduces a delocalized "donor" state at the bottom of the conduction band, yielding a metallic character. The occupied states in the conduction band (obtained integrating the total DOS in the conduction band up to the Fermi level) is 1 e^-, in agreement with the nominal "single" donor character of Al^{3+} substituting a Zn^{2+}. When a Zn atom is removed from ~~to~~ these systems (ZnSe_AlxZn+V_{Zn} and ZnTe_AlxZn+V_{Zn}) the Fermi level moves towards the top of the valence band, introducing a single "acceptor" level and giving an insulating character to the systems. The unoccupied states in the valence band (obtained integrating the total DOS from the Fermi level to the top of the valence band) is 1 e^-, in agreement with the substitution of a Zn^{2+} by an Al^{3+} and the removal of a Zn^{2+} atom. In this sense when only a Zn atom is removed from the ZnSe and ZnTe semiconductors a double "acceptor" level appears at the top of the valence band. Finally when an Al atom is replaced by a Se one (ZnSe_AlxSe) or Te one (ZnTe_AlxTe), the band gap energy disappear giving a metallic character to the system, as shown in the zoom of the Fermi level region for the ZnSe_AlxSe and ZnTe_AlxTe systems at the bottom of figure 7.

Bearing in mind these predictions and the UV-vis results, it is evident the influence of defects on the optical properties. Since an energy gap was clear observed in both semiconductors the combined presence of V_{Zn} and Al substitution is consistent with the displayed behavior.

As a first step in the prediction of the positron annihilation lifetimes τ, and before to study the doped systems we performed calculations for pure (undoped) ZnSe and ZnTe using the

experimental lattice parameters, predicting 233 and 234 ps, respectively, in agreement with the experimental values for bulk system [29]. These values are larger than τ_1 lifetime obtained in the present work, so it must be supposed that a defect having a typical lifetime below the bulk value exists [35]. For example, in ZnO, Dutta et al. [36] proposed that shallow positron traps associated to oxygen vacancies may be contributed to the first lifetime component mixed with bulk lifetime. As was already stated, mechanical work induces huge number of defects and in Zn-related semiconductors, the V_{Zn} are supposed to be single or double negatively charged, whereas the anion vacancies are assumed to be positively charged. Therefore, only the Zn vacancies are detectable by positron annihilation, but the associated lifetime value is known to be larger than the bulk lifetime. In this context, we proposed another milled generated open volume defect, i.e., that interstitial atoms (Se and Te) may contribute to reduce τ_1.

In figure 8 we show the predicted τ values for the ZnSe_AlxZn, ZnSe_AlxZn+V_{Zn}, ZnSe_V_{Zn}, and ZnSe_AlxSe (upper) and ZnTe_AlxZn, ZnTe_AlxZn+V_{Zn}, ZnTe_V_{Zn}, and ZnTe_AlxTe (bottom), as a function of the defect dilution. As shown in a previous work [23] the substitution of a Zn atom by an Al one does not modify the τ value, moreover this fact was applied to sense experimentally the dopant incorporation into the host crystalline structure [19, 20]. The substitution of an Al atom by a Se (Te) one in ZnSe (ZnTe) also does not modify substantially the τ value and converge to the values predicted for the undoped ZnSe (ZnTe) semiconductor as the dilution of the Al impurity increases. In Figure 8 the solid lines correspond to τ predicted at unrelaxed systems, i. e., at the atomic positions of the pure semiconductors. In the cases of Al doped systems without Zn vacancies ZnSe_AlxZn (ZnTe_AlxZn) and ZnSe_AlxSe (ZnTe_AlxTe) the τ predicted at unrelaxed and relaxed

systems are basically the same, and therefore not shown in figure 8. In other hand, for the systems with Zn vacancies, ZnSe_AlxZn+V_{Zn} (ZnTe_AlxZn+V_{Zn}) and ZnSe_V_{Zn} (ZnTe_V_{Zn}), τ decrease (between 4 and 5 %) when the system relaxes and achieve its equilibrium structure. In Figure 8 we show with dotted lines the behavior of the τ values for the relaxed systems. Additionally, in the systems with Zn vacancies, τ depends on the spatial distribution of the vacancy for lower dilutions (showed as stars in figure 8). As dilution increases τ converges to the values of "isolated" defects, i.e., when the defects are so diluted that do not interact with each other. The values to which τ converges are 260 ps and 275 ps for Zn vacancies in ZnSe and ZnTe, respectively. It is interesting to note that these τ values increase when the Zn vacancies decreases, showing that the Zn vacancies agglomeration increases considerably the τ value. These values agree with the observed first lifetime components, τ_1, for doped samples and those milled with surfactants. For these cases this component must include contribution not only from the bulk lifetime but also from small defects like Zn vacancies (305 and 361 ps for ZnSe and ZnTe, respectively [29]) and similar size point defects.

According to the present ab-initio calculation, the observed second lifetime component, τ_2 (> 400 ps, Table 3) contemplate larger defects like divacancies and agglomerates, in concordance with the τ_D/τ_B ratio already evaluated (Table 3). Also, a significant fraction of positrons annihilating near grain boundaries cannot be discard due to the grain size of our samples.

However, a similar theoretical analysis of τ_2 become entangled and goes beyond the goals of the present study.

Conclusions

A complete structural, optical and theoretical analysis on pure and doped Zn-based semiconductor powders prepared by mechanical milling was done. Milled samples keep their cubic crystalline structure for all milling times, showing a slight grain reduction (around 15%) for the ZnSe milled with surfactant. It is also observed that the Al dopant element was progressively incorporated into the cubic structure of both, ZnSe and ZnTe semiconductors.

Positron lifetime spectroscopy showed an increase in the value of both lifetimes due to decrease in available electron density compared to the pure semiconductor. The increase in τ_2 and τ_{av} values with the addition of surfactant indicates defect clustering near the grain boundary induced by mechanical work.

Optical data reveal all samples as direct band gap semiconductors with a slight shift to lower energy band gap (less than 2.2 eV). In our case, this shift is ascribed to the presence of defects and not to quantum size effect. From *ab initio* electronic structure study zinc vacancy (V_{Zn}) and Al substitution are the best defect choices that fixed with the exhibited semiconductor character from optical measurements.

The low-cost mechanical mill technique brought about the production of large amounts of nanostructured materials but with a high agglomeration level which cannot be avoided with surfactant addition. However, the milling process generates stress on the material that leads to formation of possible native defects, such as zinc vacancies, zinc interstitials and surface defects. Moreover, theoretical calculations allowed us to identify the different contributions to the positron annihilation lifetime and to the monotonous evolution of average lifetime.

Both positron lifetimes are strongly affected by the electronic and the structural distortions introduced by Zn vacancies and other point defects. Shallow positron traps like Se and Te interstitial are suggested to contribute to the first lifetime component. While it remains practically unperturbed when substitutional Al atoms are introduced. The variation in defect dilution confirmed the agglomeration of positron traps that leads to an increase in the second lifetime component.

The overall experimental results lead us to conclude that all samples contain great number of defects with sizes larger than a divacancy. New routes are planned to deagglomerate the obtained powders for their future technological application. Nevertheless, the obtained optical properties push this material further in the queue of optoelectronic materials to be used for applications like devices, as window layer or as absorber of UV light.

Acknowledgments

This work was supported by Consejo Nacional de Investigaciones Científicas y Técnicas (CONICET, PIP0718, 2012-2016) and Facultad de Ciencias Exactas (UNLP, 11/X772).

MM, GND and LCD are members of CONCET.

References

[1] B. Feng, J. Cao, J. Yang, S. Yang, D. Han, Characterization and photocatalytic activity of ZnSe nanoparticles synthesized by a facile solvothermal method, and the effects of different solvents on these properties, Mater. Res. Bull. 60 (2014) 794–801. https://doi.org/10.1016/j.materresbull.2014.09.071

[2] X. Li, B. Wei, J. Wang, X. Li, H. Zhai, J. Yang, Synthesis and comparison of the photocatalytic activities of ZnSe(en)0.5, ZnSe and ZnO nanosheets, J. Alloy. Compd. 689 (2016) 287–295.

[3] M.J. Kim, Y.I. Choi, S.W. Joob, M. Kang, Y. Sohn, Synthesis of Er and Yb-doped cubic and hexagonal phase ZnSe nano-assembled microspheres and their photocatalytic activities, Ceram. Int. 40 (2014)16051–16059.

[4] Rashmitha Keshav, Meghavarsha Padiyar, Meghana N, Mahesha MG. Analysis of PV deposited ZnTe thin films through Urbach tail and photoluminescence spectroscopy, Journal of Luminescence, 194, (2018), Pages 257-263.

[5] P. Ilanchezhiyan, G. Mohan Kumar, Fu Xiao, S. Poongothai, T.W. Kang, Ultrasonic-assisted synthesis of ZnTe nanostructures and their structural, electrochemical and photoelectrical properties, Ultrasonics Sonochemistry, Volume 39, November 2017, Pages 414-419.

[6] Kyoung Su Lee, Gyujin Oh, Dongil Chu, Sang Woo Pak, Eun Kyu Kim, High power conversion efficiency of intermediate band photovoltaic solar cell based on Cr-doped ZnTe, Solar Energy Materials and Solar Cells, Volume 170, October 2017, Pages 27-32.

[7] Oluwasesan Adegoke, Philani Mashazi, Tebello Nyokong, Patricia B.C. Forbes Fluorescence properties of alloyed ZnSeS quantum dots overcoated with ZnTe and ZnTe/ZnS shells, Optical Materials, Volume 54, April 2016, Pages 104-110.

[8] Rojas-Chávez, J.L. González-Domínguez, R. Román-Doval, J.M. Juárez-García, N. Daneu, Rurik Farías, ZnTe semiconductor nanoparticles: A chemical approach of the mechanochemical synthesis H., Materials Science in Semiconductor Processing 86 (2018) 128–138.

[9] Ramin Yousefi, H.R. Azimi, M.R. Mahmoudian, Wan Jeffrey Basirun, The effect of defect emissions on enhancement photocatalytic performance of ZnSe QDs and ZnSe/rGO nanocomposites, Applied Surface Science 435 (2018) 886–893.

[10] Marcela Achimovičová, Zdenka Bujňáková, Martin Fabián and Anna Zorkovská, Study of de-aggregation of mechanochemically synthesized ZnSe nanoparticles by re-milling in the presence of $ZnCl_2$ solution, Acta Montanistica Slovaca Ročník 18 (2013), číslo 2, 119-124.

[11] M. Shobana, S.R. Meher, Experimental and ab-initio study of the structural, electronic and vibrational properties of ZnTe, Journal of Alloys and Compounds 762 (2018) 260-271.

[12] A.F. Qasrawi, Ansam M. Alsabe, Engineering the structural, optical and dielectric properties of ZnSe thin films via aluminum nano-sandwiching, Optik 198, (2019), 163295.

[13] Daotong YouChunxiang XuWei ZhangJie ZhaoFeifei QinZengliang Shi, Photovoltaic-pyroelectric effect coupled broadband photodetector in self-powered ZnO/ZnTe core/shell nanorod arrays, Nano Energy 62, (2019), 310-318.

[14] Yijie WangMin ZhongWu WangQiuyu WangWenduo WuXingchuan Luo, Effects of ZnSe modification on the perovskite films and perovskite solar cells based on ZnO nanorod arrays, Applied Surface Science, 495 (2019) 143552. https://doi.org/10.1016/j.apsusc.2019.143552.

[15] Yicheng Wang, Honglai Li, Tiefeng Yang, Zixing Zou, Zhaoyang Qi, Liang Ma, Junying Chen, Space-confined physical vapour deposition of high quality ZnTe nanosheets for optoelectronic application, Materials Letters 238 (2019) 309–312.

[16] Muhammad Arshad Kamran, Novel low-temperature synthesis and optical properties of 1D-ZnTe nanowires, Journal of Science: Advanced Materials and, Devices 3 (2018), 226-229, https://doi.org/10.1016/j.jsamd.2018.04.001.

[17] Shunji OzakiKazuya Matsumoto, Growth of ZnSe nanowires on quartz substrates and their photo modulated transmittance spectra, Journal of Physics and Chemistry of Solids, 127, (2019), 115-118.

[18] C.Suryanarayana, E.Ivanov, Mechanochemical synthesis of nanocrystalline metal powders, Advances in Powder Metallurgy Properties, Processing and Applications, Woodhead Publishing Series in Metals and Surface Engineering, 2013, Pages 42-68. https://doi.org/10.1533/9780857098900.1.42.

[19] L.C. Damonte, V. Donderis, S. Ferrari, M. Meyer, J. Orozco, and M.A. Hernandez Fenollosa. ZnO-based nanocrystalline powders with applications in hybrid photovoltaic cells. International Journal of Hydrogen Energy, 35:5834–5837, 2010.

[20] L.C. Damonte, J. Orozco, S. Ferrari and M.A. Hernandez Fenollosa. Al-doped ZnO mechanical milled powders for dye sensitized cells. Journal of Alloys and Compounds · April 2010.

[21] J. Hoya, J.I. Laborde, L.C. Damonte, Structural characterization of mechanical milled ZnSe and ZnTe powders for photovoltaic devices, Int.J.Hydrogen Energy 37 (2012) 14769-14772.

[22] J.I. Laborde, J. Hoya, M.D. Reyes Tolosa, M.A. Hernández-Fenollosa, L.C. Damonte, Mechanical milled doped Zn-based semiconductors powders for photovoltaic devices, Int.J.Hydrogen Energy 39 (2014) 8697-8701.

[23] L.C. Damonte, G. N. Darriba, M. Rentería Structural and electronic properties of Al-doped ZnO semiconductor nanopowders: Interplay between XRD and PALS experiments and first-principles/DFT modeling. Journal of Alloys and Compounds 735 (2018) 2471–2478.

[24] P. Blaha, K. Schwarz, G. Madsen, D. Kvasnicka, J. Luitz,"WIEN2k, An Augmented Plane Wave Plus Local Orbitals Program for Calculating Crystal Properties", Technical Universität, Wien, Austria (2012).

[25] J.P. Perdew, Y. Wang, Phys. Rev. B 45 (1992) 13244-13249

[26] T. Torsti, M. Heiskanen, M.J. Puska, R.M. Nieminen, Int. J. Quantum Chem., 91 (2003) 171-176

[27] Kirkegaard P, Pedersen NJ, Eldrup M. PATFIT-88 Riso-M-2740; 1989. Risø.

[28] Qiang Fu and Wenbo Sun, Mie theory for light scattering by a spherical particle in an absorbing medium, Applied Optics Vol. 40, Issue 9, pp. 1354-1361 (2001) https://doi.org/10.1364/AO.40.001354.

[29] G. Tessaro, P. Mascher, Point defect characterization of Zn- and Cd-based semiconductors using positron lifetime spectroscopy, Journal of Crystal Growth 197 (1999) 581-585.

[30] L.C. Damonte, V. Donderis, S. Ferrari, J. Orozco, M.A. Hernández-Fenollosa, Al-doped ZnO mechanical milled powders for dye sensitized cells, Journal of Alloys and Compounds 495 (2010) 432–435, doi:10.1016/j.jallcom.2009.11.057.

[31] J. Tauc, Amorphous and Liquid Semiconductors, Springer US, Boston, MA, 1974. doi:10.1007/978-1-4615-8705-7.

[32] Shashikant RajpalS.R. Kumar, Thermoluminescent properties of nanocrystalline ZnTe thinfilms: Structural and morphological studies, Physica B: Condensed Matter (2018) 145-149. https://doi.org/10.1016/j.physb.2018.01.046

[33] M.J. Puska, R.M. Nieminen, J. Phys. F: Met. Phys. 13 (1983) 333-346

[34] E. Boronsky, R.M. Nieminen, Phys. Rev. B 34 (1986) 3820-3831.

[35] R. Krause-Rehberg, H.S. Leipner, T. Abgarjan, A. Polity; Review of defect investigations by means of positron annihilation in II−VI compound semiconductors, Appl. Phys. A 66, 599–614 (1998).

[36] Sreetama Dutta, S. Chattopadhyay, A. Sarkar, Mahuya Chakrabarti, D. Sanyal, D. Jana; Role of defects in tailoring structural, electrical and optical properties of ZnO, Progress in Materials Science 54 (2009) 89–136.

Figure Captions

Figure 1. XRD patterns for ZnSe powders. a) pure ZnSe after 10 hours of milling without surfactant, b) ZnSe after 1 and 10 hours of milling with $ZnCl_2$, c) ZnSe 30 hours of milling with methanol. d) ZnSe with Al after 1 and 10 hours of milling without surfactant,

Figure 2. XRD patterns for ZnTe powders. a) pure ZnTe after 10 hours of milling without surfactant, b) ZnTe after 1 and 10 hours of milling with $ZnCl_2$, c) ZnTe 30 hours of milling with methanol, d) ZnTe with Al after 1 and 10 hours of milling without surfactant,.

Figure 3. SEM images for Al:ZnSe (left) after 10 hours of milling

Figure 4. Average positron lifetime for all the powder samples. Triangle ZnTe samples and circle ZnSe samples.

Figure 5. Absorbance spectra for a) ZnSe powders with different surfactants, up empty triangle 10%$ZnCl_2$, up full triangle 3%$ZnCl_2$ and down triangle Methanol. b) ZnTe powder samples, circle pure ZnTe, triangle with 10% $ZnCl_2$ addition and square with 5at% Al.

Figure 6. Tau-Mot plots for a) ZnSe powders with different surfactants, up empty triangle 10%$ZnCl_2$, up full triangle 3%$ZnCl_2$ and down triangle Methanol. b) ZnTe powder samples, circle pure ZnTe, triangle with 10% $ZnCl_2$ addition and square with 5at% Al.

Figure 7. Total electronic density of states (DOS) for left (from top to bottom): undoped ZnSe, replacing one Zn atom by one Al atom in ZnSe (ZnSe_AlxZn), replacing one Zn atom by one Al atom and removing one Zn atom in ZnSe (ZnSe_AlxZn+VZn), removing one Zn atom in ZnSe (ZnSe_VZn), and replacing one Se atom by one Al atom in ZnSe (ZnSe_AlxSe). Right (from top to bottom): undoped ZnTe, replacing one Zn atom by one Al atom in ZnTe (ZnTe_AlxZn), replacing one Zn atom by one Al atom and removing one Zn atom in ZnTe (ZnTe_AlxZn+VZn), removing one Zn atom in ZnTe (ZnTe_VZn), and replacing one Te atom by one Al atom in ZnTe (ZnTe_AlxTe).

Figure 8. Positron annihilation life time τ predicted for different defects in ZnSe (up) and ZnTe (down) as a function of the defect dilution. The horizontal dotted line is the predicted value for pure ZnSe (up) and ZnTe (down) bulk systems. The dotted curves correspond to τ values predicted at relaxed systems. In both pictures the star correspond to τ values predicted for different Zn vacancies distribution, the closed (open) star correspond to unrelaxed (relaxed) systems.

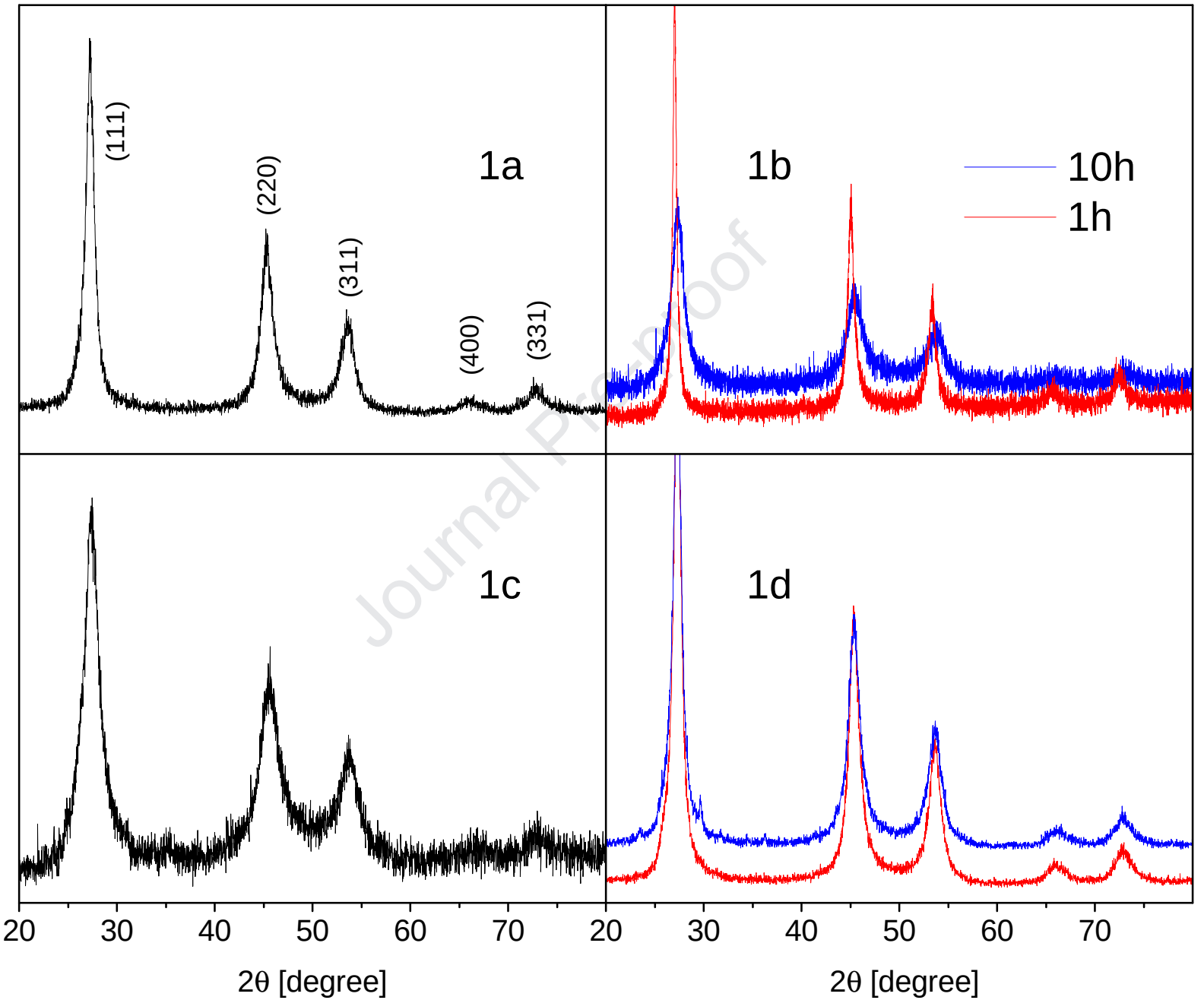

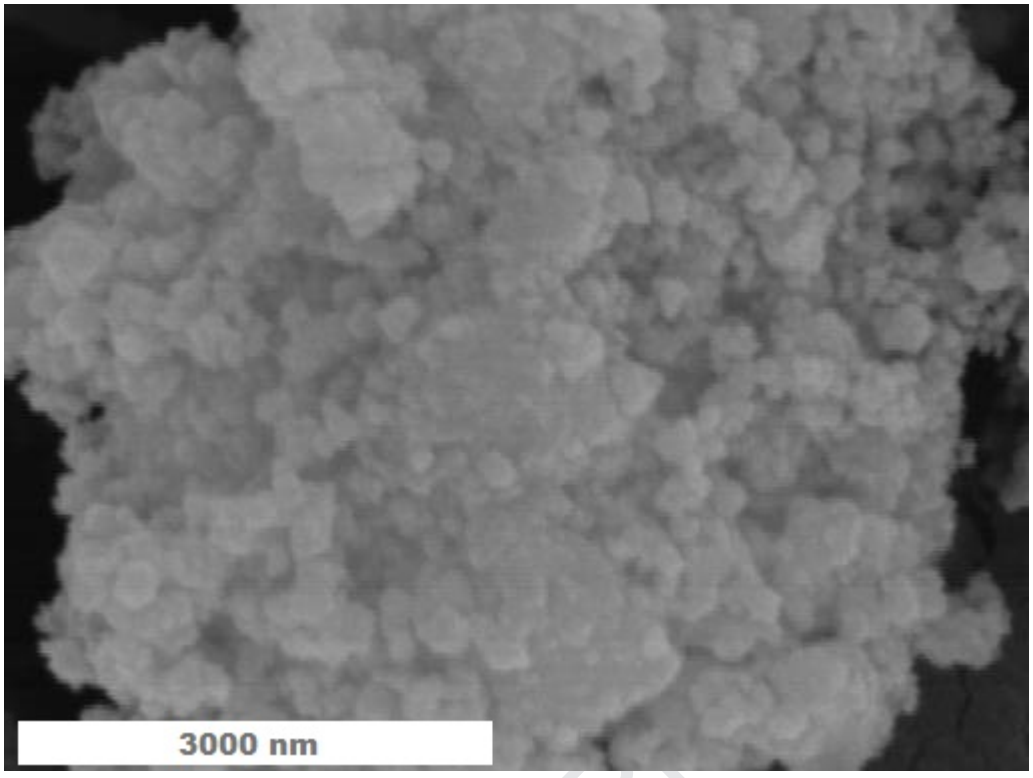

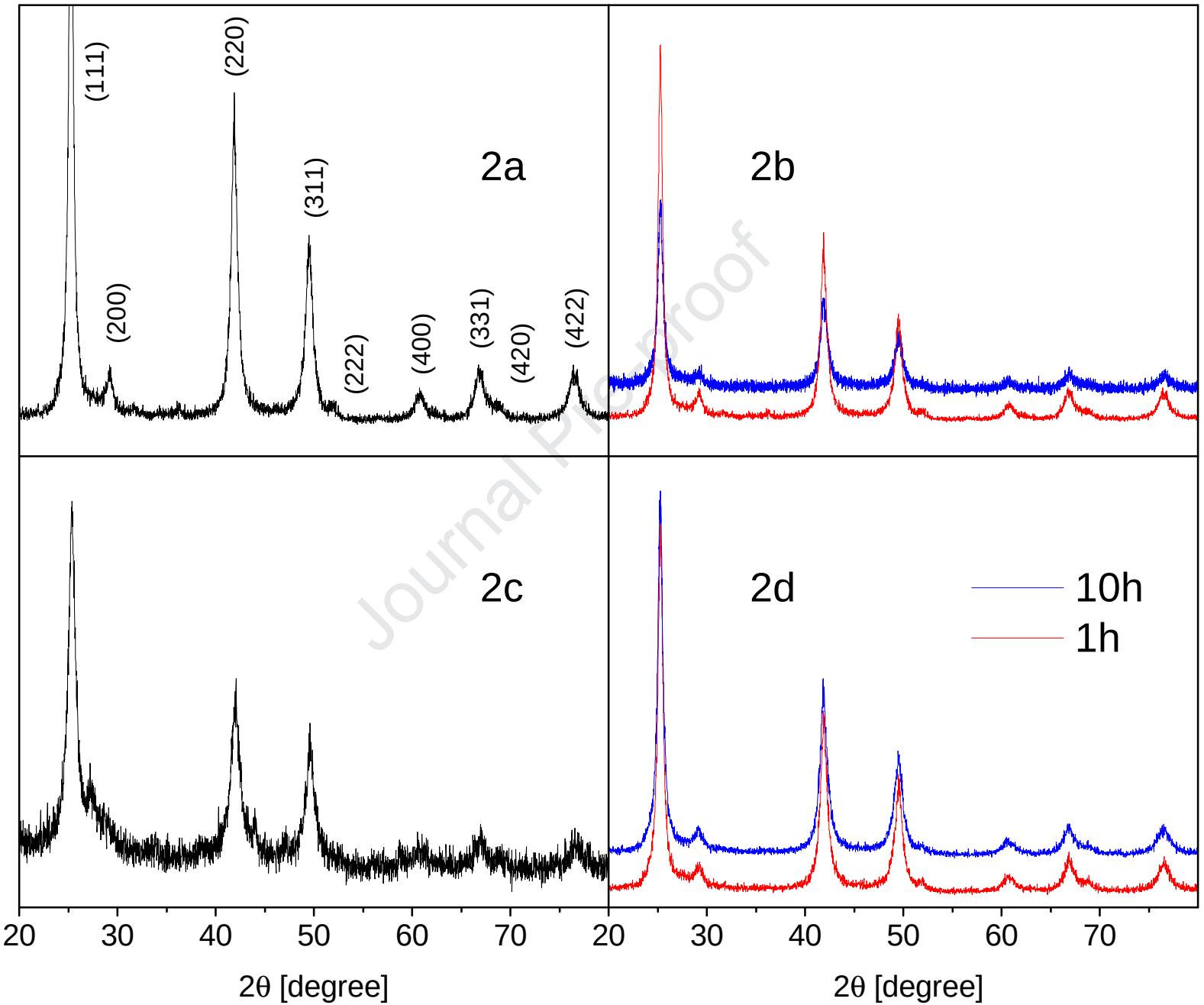

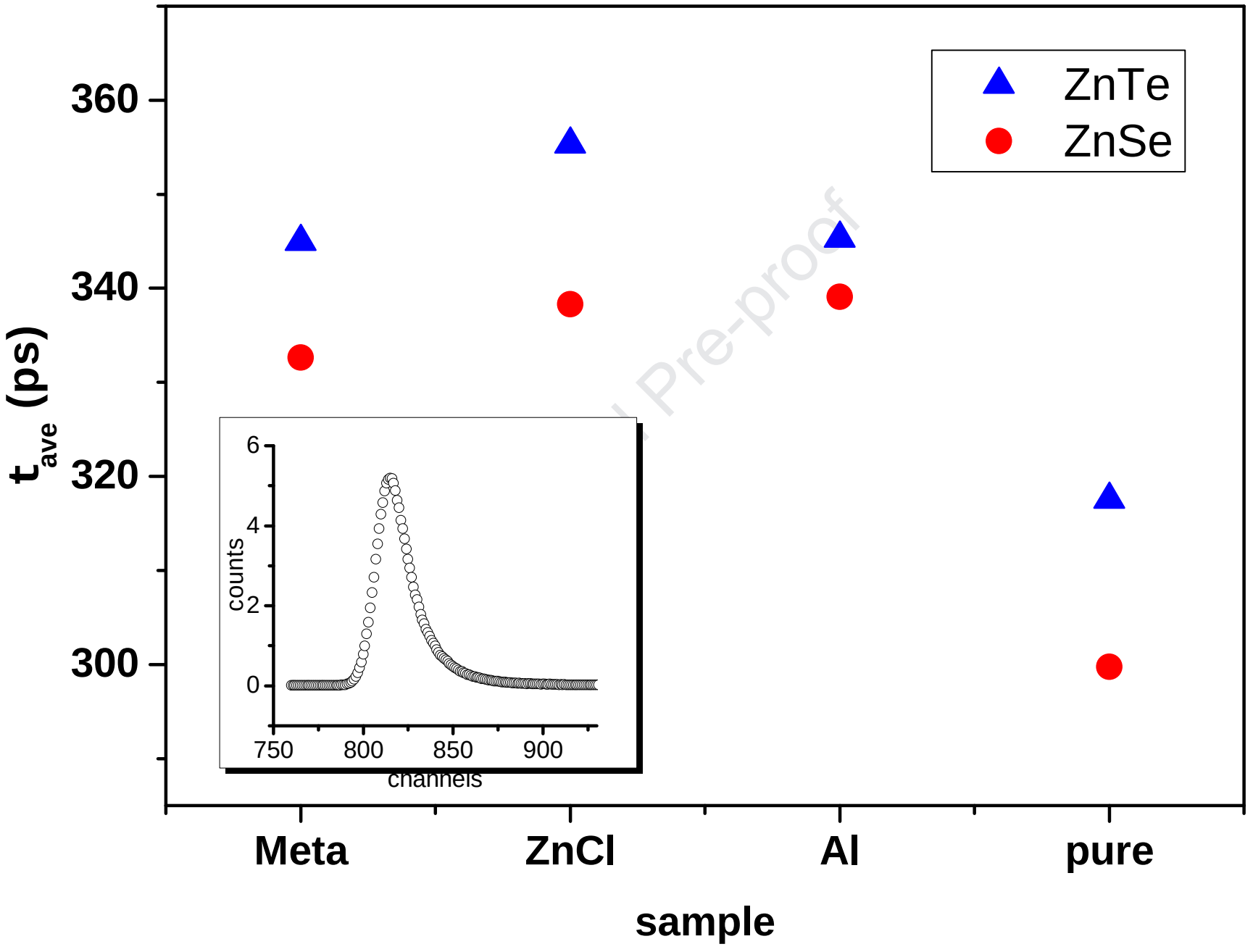

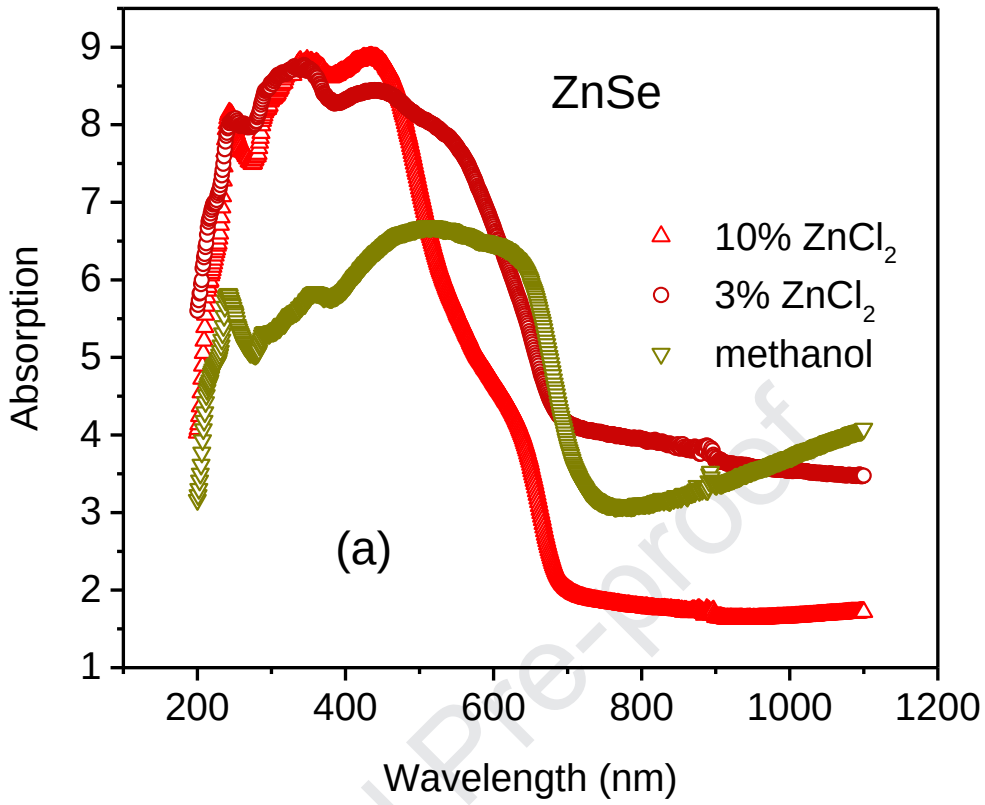

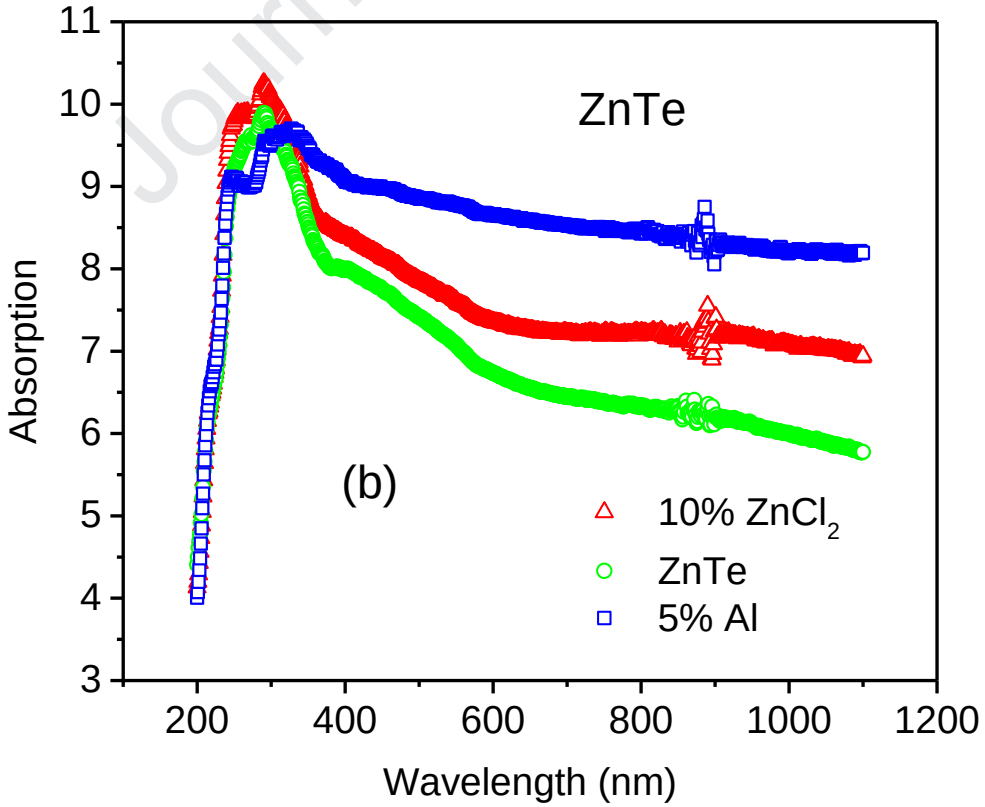

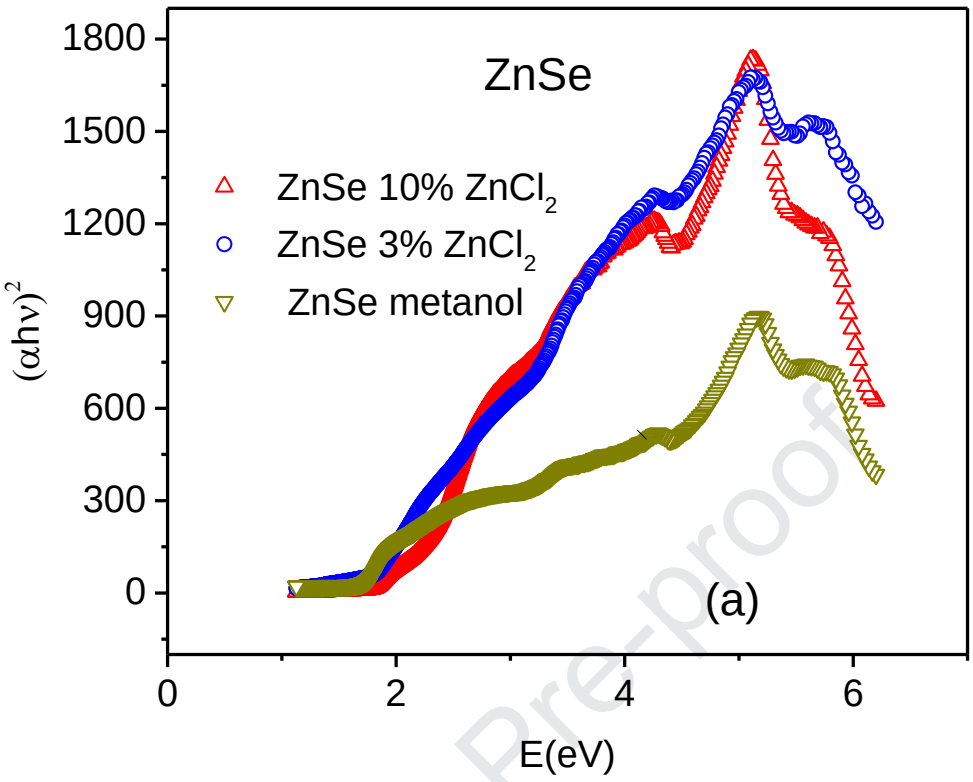

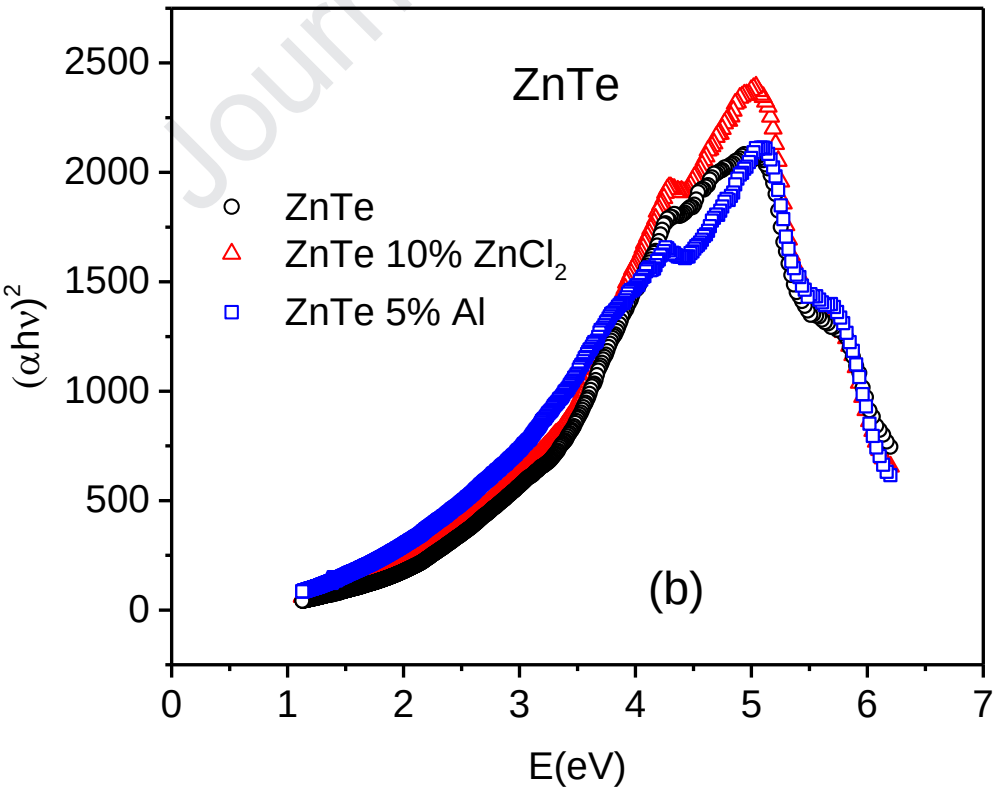

Figure 7

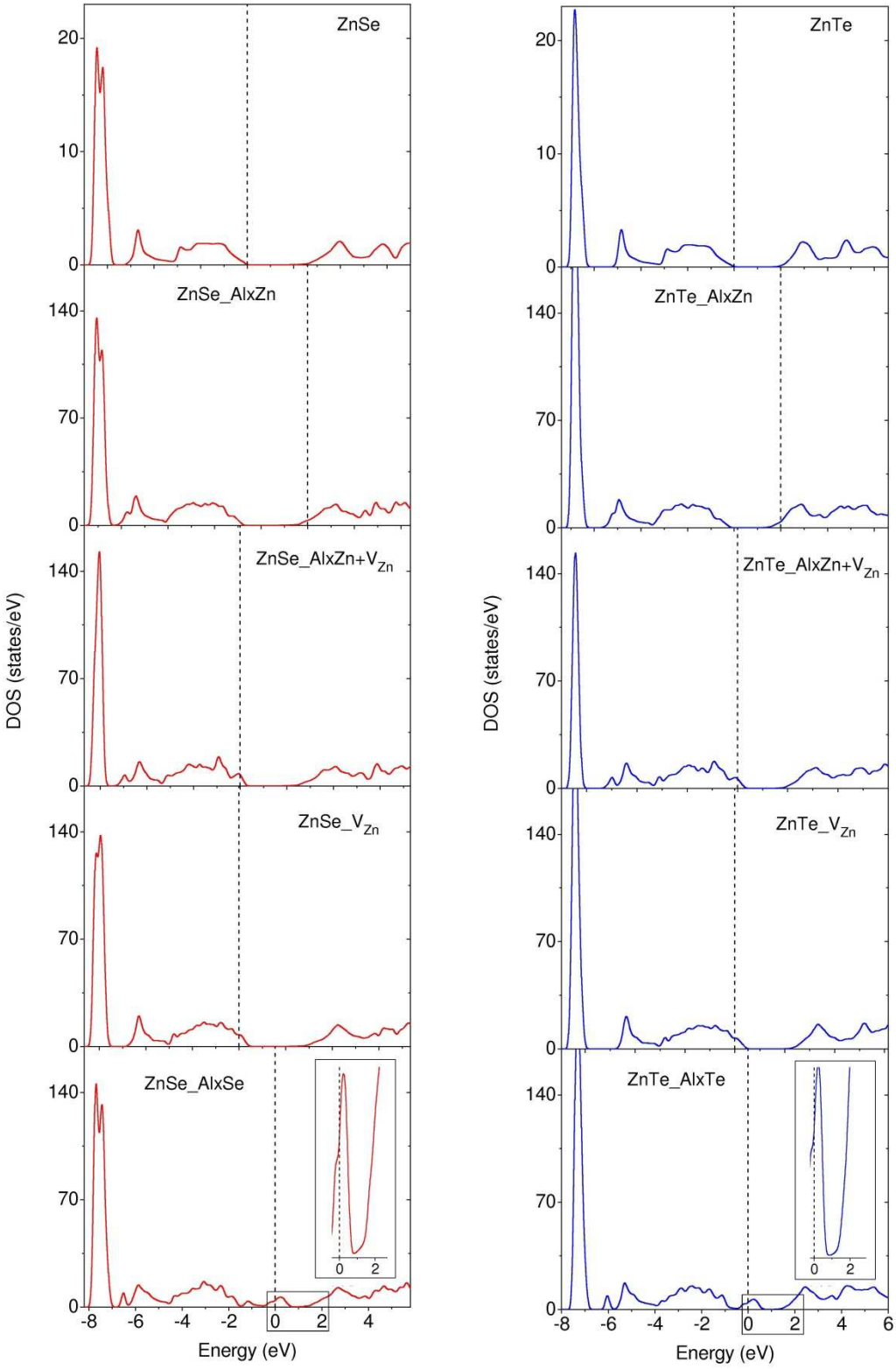
ZnSe
ZnSe_AlxZn
ZnSe_AlxZn+V$_{Zn}$
ZnSe_V$_{Zn}$
ZnSe_AlxSe
ZnTe
ZnTe_AlxZn
ZnTe_AlxZn+V$_{Zn}$
ZnTe_V$_{Zn}$
ZnTe_AlxTe
DOS (states/eV)
Energy (eV)

Figure 8

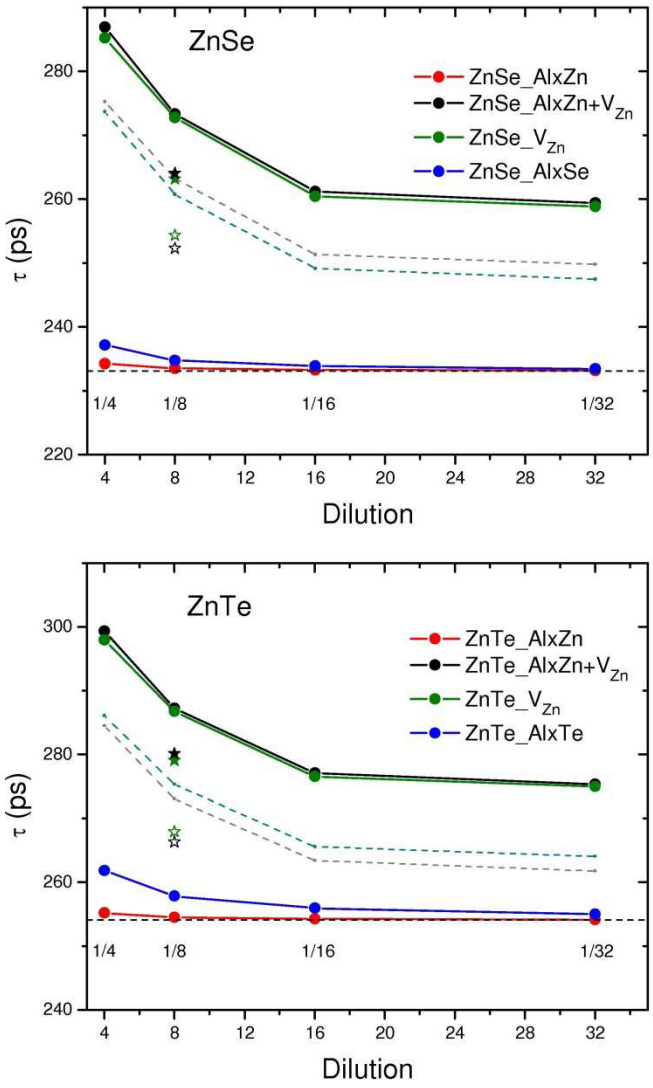
ZnSe
ZnSe_AlxZn
ZnSe_AlxZn+V_Zn
ZnSe_V_Zn
ZnSe_AlxSe
τ (ps)
280
260
240
220
1/4
1/8
1/16
1/32
4
8
12
16
20
24
28
32
Dilution
ZnTe
ZnTe_AlxZn
ZnTe_AlxZn+V_Zn
ZnTe_V_Zn
ZnTe_AlxTe
τ (ps)
300
280
260
240
1/4
1/8
1/16
1/32
4
8
12
16
20
24
28
32
Dilution

Highlights for "*Surfactant and dopant addition effect on optical and structural properties of ZnSe (Te) nanostructured semiconductors"*

ZnSe (Te) nanostructured semiconductors prepared by mechanical milling

The addition of surfactant does not avoid the agglomeration of particles

Al incorporation leads to a slight shift of energy bandgap

Density of State were predicted by ab initio calculations

The presence of defects is necessary to maintain the semiconductor character

Positron traps are interpreted in terms of the theoretical approach

Declaration of interests

☒ The authors declare that they have no known competing financial interests or personal relationships that could have appeared to influence the work reported in this paper.

☐The authors declare the following financial interests/personal relationships which may be considered as potential competing interests: